reactions

MDPI

Article

Synergistic Pd-La Catalysts on ATO for Clean Conversion of Methane into Methanol and Electricity

Paulo Victor. R. Gomes, Dolores R. R. Lazar, Gabriel Silvestrin, Victoria Amatheus Maia, Rodrigo Fernando B. de Souza and Almir Oliveira Neto *

IPEN—CCCH (Células a Combustível e Hidrogênio), Cidade Universitária, Av. Professor Lineu Prestes, 2242, São Paulo 05508-000, SP, Brazil; drlazar@usp.br (D.R.R.L.); gabrielsilver2001@gmail.com (G.S.); victoriaamaia@usp.br (V.A.M.); souza.rfb@gmail.com (R.F.B.d.S.)
* Correspondence: aolivei@usp.br

Abstract: This study investigates the electrochemical conversion of methane to methanol using fuel-cell-type reactors with palladium- and lanthanum-based catalysts supported on antimony-doped tin oxide (ATO). The combination of these elements demonstrated promising characteristics for selective methanol production. Transmission electron microscopy (TEM) analysis revealed the impact of lanthanum addition on palladium nanoparticles, influencing size distribution and clusters. Polarization curves and power density plots highlighted the $Pd_{50}La_{50}$/ATO catalyst, indicating an optimal palladium/lanthanum ratio for methanol optimization. FTIR analysis confirmed the presence of methanol in the reaction products, while the methanol production rate showcased the superior performance of the $Pd_{50}La_{50}$/ATO catalyst compared to other compositions. The synergistic effects between lanthanum's water activation capability and the carbophilic nature of PdO emerged as crucial factors for the catalyst's success.

Keywords: ATO; PEM fuel cell; methanol; catalysis

Academic Editor: Ioannis V. Yentekakis

Received: 23 October 2024
Revised: 12 December 2024
Accepted: 23 December 2024
Published: 3 January 2025

Citation: Gomes, P.V.R.; Lazar, D.R.R.; Silvestrin, G.; Maia, V.A.; de Souza, R.F.B.; Neto, A.O. Synergistic Pd-La Catalysts on ATO for Clean Conversion of Methane into Methanol and Electricity. *Reactions* **2025**, *6*, 2. https://doi.org/10.3390/reactions6010002

1. Introduction

Methane, long regarded as a clean energy source, aligns with the growing demand for energy, particularly cleaner and more sustainable options. However, when used as a conventional energy source, methane's combustion results in the emission of an amount of CO_2 equivalent to the methane consumed [1–3]. Moreover, methane is a greenhouse gas more potent than CO_2 when present in the atmosphere. Thus, the pursuit of means to mitigate its emissions represents a significant advancement [3–10].

One alternative involves converting methane, an abundant hydrocarbon source, into industrially relevant chemicals, with methanol being an attractive option due to its applications as a solvent, fuel, disinfectant, and synthesis precursor. Various pathways for methane to methanol conversion have been explored, including homogeneous catalysis, photocatalysis, biocatalysis, plasma technologies, and electrochemical routes [6–14]. Electrochemical processes emerge as promising, especially those characterized by the co-generation of chemicals and electricity [6]. In this context, the use of polymer electrolyte fuel cells as reactors for methane conversion has been studied, showing significant potential to operate under mild conditions and achieve the desired conversion [14–21].

However, the intricacy of this obstacle stems from the inherent resistance posed by the C-H bond (434 kJ mol^{-1}) in methane, coupled with its low polarizability, rendering the oxidation of methane a formidable undertaking [20,22]. To surmount this challenge, investigators have pursued an alternative strategy that entails the indirect oxidation of

methane. This involves activating methane with more reactive species generated through Faradaic processes, specifically oxygenated reactive species (ROS) originating from the activation of water in an electrochemical reaction [5,18].

Pd has been identified in the literature as a crucial metal for methane adsorption and increased catalytic activity in the reaction. However, it typically needs to be associated with another transition metal that facilitates water activation, such as Ni, Cu, or Sb, among others [12,13,15,19]. Lanthanum, when used in conjunction with other metals, acts as a catalyst, aiming to improve water resistance in these materials, enhance oxygen storage capacity, and improve the interaction between active species and support [6,11].

For electrocatalysis in the methane-to-methanol conversion, the catalyst must possess specific characteristics, including the bifunctional capacity to adsorb methane and activate water molecules [2]. Additionally, the support for these materials must be resistant to corrosion by reactive oxygen species. In this context, metallic oxides like TiO_2 or antimony-doped tin oxide (ATO) have emerged as promising catalytic supports. Among these options, ATO has been strategically chosen due to its tendency to form oxygenated reactive species, as well as its notable properties of electrical conductivity and corrosion resistance [23]. This choice makes ATO a viable and effective option as a catalytic support for the methane-to-methanol conversion reaction [9]. It is known that the radical reaction promoted by ROS is poorly selective and can lead hydrocarbons to more oxidized molecules. Therefore, modulating the optimal amount of ROS to obtain more methanol rather than CO_2 or formates is highly recommended. We discovered that this modulation can be achieved not only through the operating potential but also through the catalytic material composition. These ROS, which tend to be corrosive, are responsible for methane conversion. Finally, ATO provides stability to the catalyst by preventing further agglomeration of catalytic particles and protecting them from additional oxidative processes caused by ROS.

In this study, we demonstrate the activity of adding La to Pd supported on ATO for the conversion of methane into methanol.

2. Methods

The PdLa/ATO materials were produced by a sodium borohydride reduction method [4] with varying atomic ratios. In the preparation process, a mixture of ultrapure water and isopropanol (50/50 *v*/*v*) was ultrasonically bathed with a specific quantity of ATO support (Sb_2O_5•SnO_2 Aldrich (Sigma-Aldrich, Milwaukee, WI, USA)) for 15 min. After, metallic precursors $Pd(NO_3)_2$•2 H_2O (Aldrich) and $LaCl_3$• H_2O (Aldrich) in different atomic ratios (20%) were added to the solution. $NaBH_4$ (Aldrich) was then added to a 10 mL 0.01 mol L^{-1} NaOH solution with a 5:1 excess in relation to the metals, and stirring was maintained for 30 min. The synthesized material underwent washing and filtration using 4.0 L of ultrapure water.

Transmission electron microscopy (TEM) with a JEOL JEM-2100 (JEOL, Tokyo, Japan) at 200 keV was employed to examine the morphology of PdLa/ATO materials. ImageJ software (Version 1.54m) analyzed the size of 300 nanoparticles for each catalyst, generating histograms. X-ray Diffraction (XRD), utilizing a Rigaku Miniflex II diffractometer (Rigaku, Tokyo, Japan) with Cu/k$\alpha\lambda$ = 0.154 nm, covered the 2θ range from 20 to 90° at a scan speed of 2° min^{-1}. Cyclic voltammetry experiments utilized a three-electrode cell setup with a PdLa/ATO working electrode, a Pt plate counter electrode (2 cm^2), and a commercial Ag/AgCl (3.0 mol L^{-1} KCl) reference electrode. In situ Raman analysis utilized a Raman Microspectrometer with a 785 nm laser.

A Proton Exchange Membrane (PEM) fuel cell reactor assembled with a PdLa-catalyst-containing anode, similar to that used in previous studies [4,18,23], operated under a methane flow of 300 mL min^{-1} and a 1.0 mol L^{-1} NaOH solution at 1.0 mL min^{-1}. The

cathode received humidified O_2 (200 mL min^{-1}) at 85 °C. Reaction products were collected and analyzed via infrared spectroscopy (Nicolett® 6700 (Thermo Fisher Scientific, Waltham, MA, USA)) and HPLC (YL9100) at intervals from the open circuit potential to 0.0 V. The calibration curve for methanol analysis showed a peak area = 0.29574 + 0.00979 [methanol] with r^2 = 0.994. HPLC analysis employed a C18 (Phenomenex Luna (Phenomenex, Torrance, CA, USA) 5 µm, 250 × 4.6 nm) column with a flow of 0.8 mL min^{-1} containing 50% water, 40% acetonitrile, and 10% buffer solution in an isocratic run.

3. Results and Discussion

Transmission electron microscopy (TEM) was utilized to analyze the particle size distribution of PdLa catalysts supported on ATO, as depicted in Figure 1. The results reveal that increasing the lanthanum content leads to a higher number of visible clusters, a trend reminiscent of the effects observed when incorporating other rare-earth elements into noble metal nanoparticles, such as PtCe/C [1]. This increase is clearly depicted in the histograms, where it was observed that, at varying compositions, the average nanoparticle size ranges between 7.0 and 9.0 nm. Specifically, the smallest average size was recorded for $Pd_{80}La_{20}$/ATO, while the largest was observed for La/ATO. This finding suggests that the lanthanum content significantly influences the particle size distribution of the catalyst, with implications for its catalytic performance.

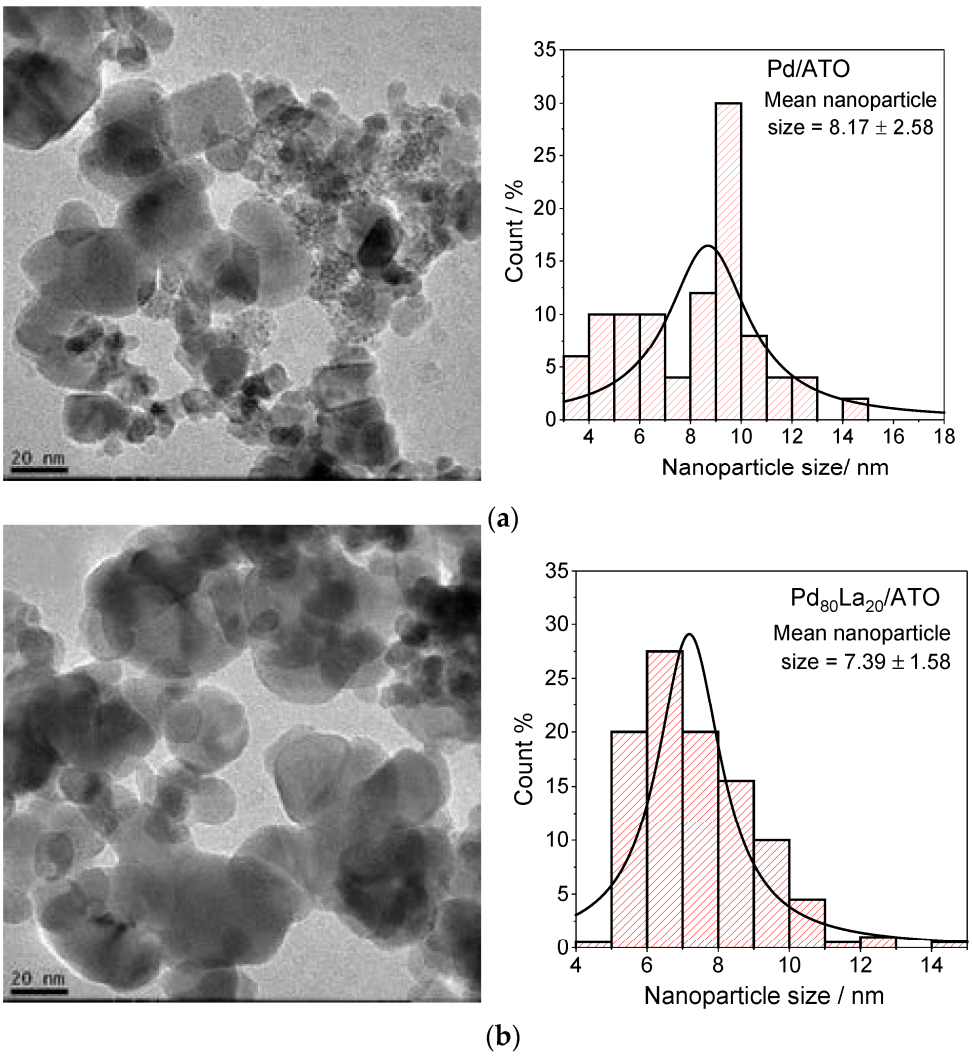

Figure 1. *Cont.*

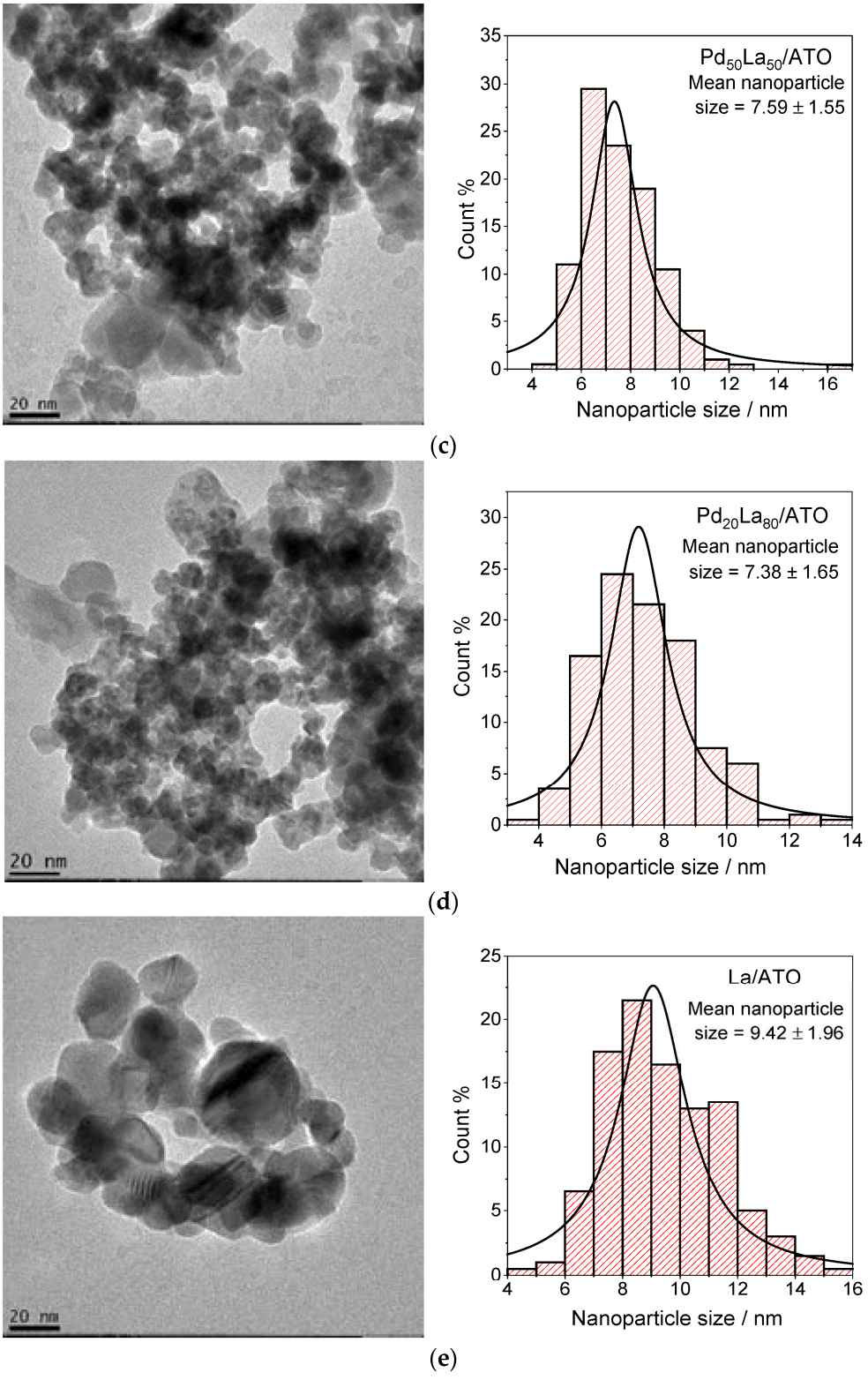

Figure 1. Transmission electron microscopy (TEM) micrograph and histograms of nanoparticle size distribution for (**a**) Pd/ATO, (**b**) $Pd_{80}La_{20}$/ATO, (**c**) $Pd_{50}La_{50}$/ATO, (**d**) $Pd_{20}La_{80}$/ATO, and (**e**) La/ATO.

Figure 2 shows the X-ray diffractogram patterns of Pd/ATO, PdLa/ATO, and La/ATO electrocatalysts. The identified peaks at $2\theta \approx 26°$, 33°, 38°, 51°, 54°, 62°, and 64° correspond to characteristic diffraction peaks of ATO (JCPDS# 88-2348). Notably, the palladium peaks appear subtly against the background of ATO peaks. Normalizing the diffraction pattern

intensity with a logarithmic function (Figure 2b) brings forth the distinctive peaks of Pd and La. Pd-related peaks at $2\theta \approx 38^\circ$, 49°, and 66°, corresponding to the crystalline planes (111), (200), (220), and (311) according to (JCPDS# 89-4897), confirm a face-centered cubic (FCC) structure for Pd/ATO. Additionally, La_2O_3-related peaks (JCPDS no. 05-0602) are discerned at ~28, 47, 56, and 72°.

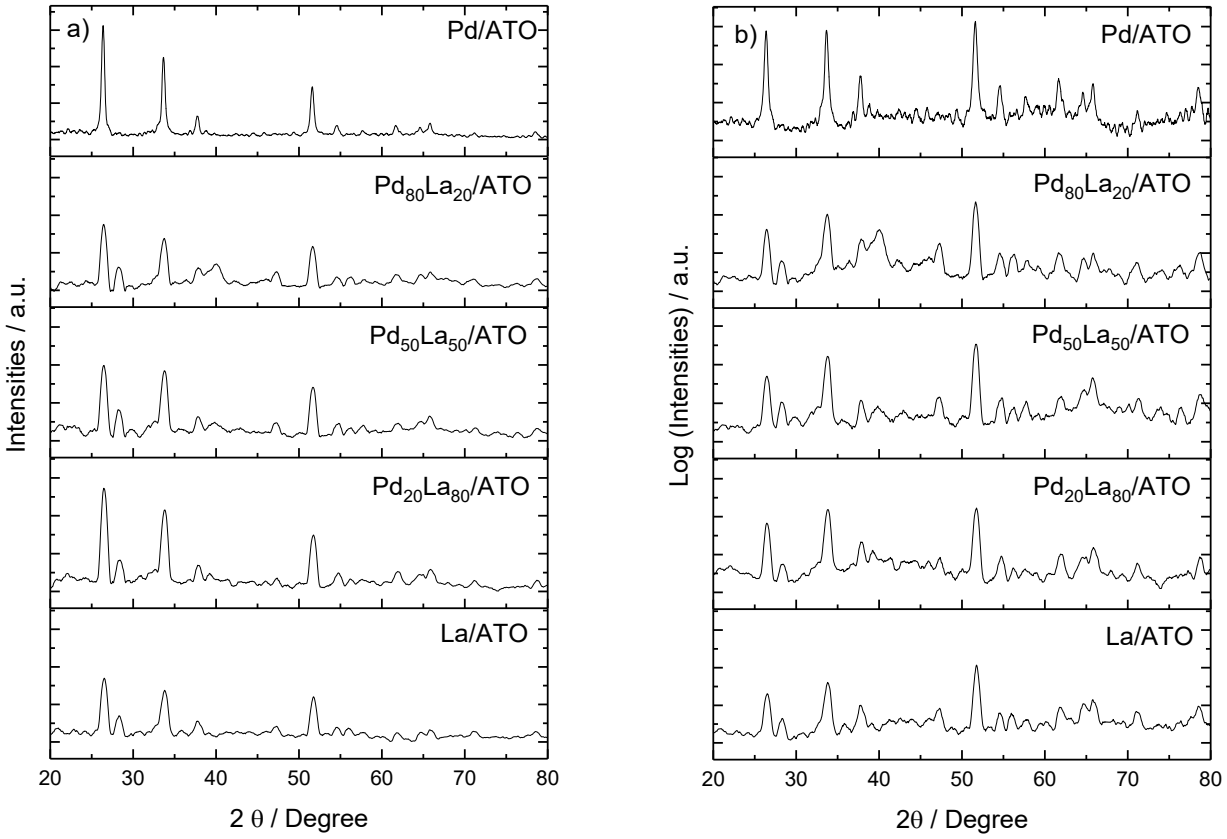

Figure 2. X-ray diffractogram patterns of Pd and La catalysts supported on ATO in various ratios, with panel (**a**) depicting the XRD pattern and panel (**b**) presenting the XRD pattern with intensities normalized by the logarithmic function.

To examine the material's performance under conditions mirroring practical applications, cyclic voltammetry coupled with in situ Raman spectroscopy was employed. In Figure 3a, cyclic voltammograms of PdLa materials in different ratios are depicted. Materials containing Pd exhibit oxidation/desorption peaks between −0.8 and −0.5 V during the positive scan, followed by a reduction/adsorption profile starting from −0.6 V [6]. It is noteworthy that in cyclic voltammetry, the region of hydrogen adsorption/desorption becomes less clear with increasing La content due to the synergistic effects of metallic oxides present, which can potentially block the palladium surface [17].

The interaction between methane and PdO is weak and does not significantly alter the current profile or density, which is why it is not presented. The predominant process depends only on the activation of water. In addition, the solubility of methane in water is very low, so we are looking for other types of electrochemical reactors to study the oxidation of methane, such as the fuel-cell-type reactor, built for the gaseous reaction due to the region where solid, liquid, and gas are present and reactive simultaneously.

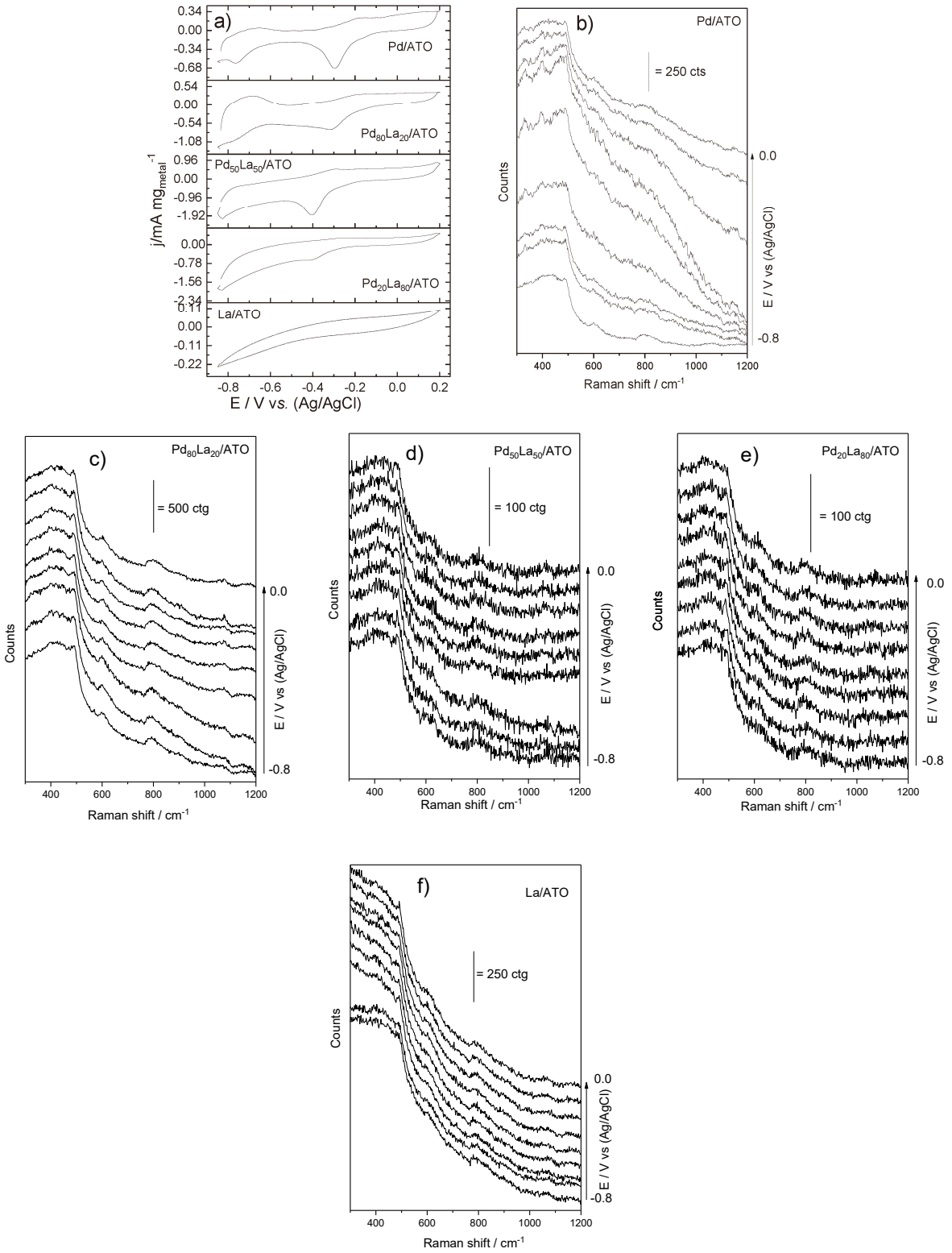

Figure 3. Cyclic voltammetry coupled with in situ Raman spectroscopy (**a**) CV of La/ATO, Pd/ATO, and PdLa/ATO in different ratios (scan rate v = 10 mV s^{-1}) in a 1.0 mol L^{-1} NaOH aqueous solution. Additionally, panels (**b**–**f**) showcase spectra of Raman-assisted electrochemical measurements collected at −0.85 at 0.2 V during CV experiment.

For further insights into the electrochemical processes promoting partial methane oxidation and the interaction between the catalyst and the electrolyte, electrocatalytic activity analysis was performed in situ with Raman spectroscopy, as indicated in Figure 3b–f). The

Raman spectra reported bands in the range of 300 to 1200 cm^{-1}. Distinctive bands of SnO_2 are identified at approximately 486, 602, and 780–793 cm^{-1} [15,23,24], representing the active bands of SnO_2 Eg, A1g, and B2g, respectively. In Pd-containing materials, the band at 638 cm^{-1} exhibits heightened intensity and width, indicating a convolution of the Eg mode of TiO_2 torsion of the PdO-H bond at 637cm^{-1} [16]. Bands below 500 cm^{-1} are likely attributed to La-O vibrations, showing an increasing trend with a shift to less positive potentials. It is observed that the increase in the La-O band diminishes the definition of the PdO-H band, both by shifting towards less negative potentials and by the increase in lanthanum concentration. This is due to the oxygen buffering nature of rare-earth elements, which should hinder the formation of PdO-H, as well as steric hindrance of sites. Additionally, the Nafion bands appear at 794, 974, and 1166 cm^{-1} [7,8].

In Figure 4, the polarization curves for the electrochemical methane conversion in a polymeric reactor using PdLa/ATO anodic catalysts in different compositions are presented. The obtained open-circuit potential (OCP) values ranged from 0.25 to 0.50 V, consistent with the literature findings for similar reactors [6,19], except for the $Pd_{20}La_{80}$/ATO catalyst, which exhibited an OCP of 0.15 V. The highest OCP value was observed for the $Pd_{50}La_{50}$/ATO catalyst, corresponding to the highest power density of approximately ~1.3 mW cm^{-2}.

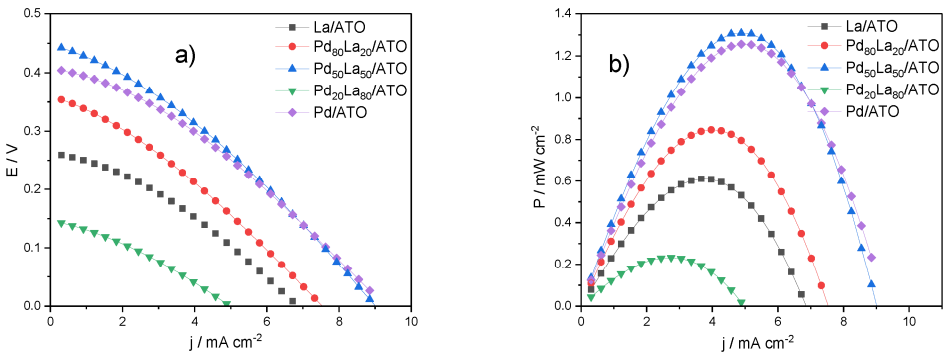

Figure 4. Polarization curves for electrochemical methane conversion (**a**) E/j curves of PdLa/ATO in various compositions. (**b**) Power density curves. (**a**) Illustrations of polarization curves for PdLa supported on ATO.

The incorporation of lanthanum with palladium was undertaken, as the fluctuation in lanthanum content relative to palladium did not result in a higher open-circuit potential and power density compared to the $Pd_{50}La_{50}$/ATO catalyst. This observation might be associated with a mechanism favoring the generation of methane oxidation products through oxygenated reactive species [18]. Furthermore, the distribution of nanoparticles across the catalyst surface may facilitate their oxidation by palladium. This phenomenon could contribute to an elevation in the open-circuit potential, given that the oxidation potentials of methanol and formic acid are lower than the water activation potential.

The FTIR spectra presented in Figure 5 were obtained through the analysis of aliquots collected every 100 mV over the reactor's operation for 5.0 min. The band observed at ~1304 cm^{-1} is characteristic of methane, indicating the dissolution of the gas in the aqueous medium [19], indicative of an increase in organic species in solution. Meanwhile, bands related to methanol are observed at 1033, 1077, and 1082 cm^{-1} [9], more prominently in the Pd/ATO and $Pd_{80}La_{20}$/ATO materials. Bands at ~1340 cm^{-1}, corresponding to formate [4], were also found in all materials, indicating that the oxidative process leading to methanol formation ultimately produces other more-oxidized products. For $Pd_{80}La_{20}$/ATO, methanol production occurred at 0.2 V, but with a higher presence of formate, as observed in the FTIR spectra, which may have masked the detection and prevented it from being

accurately reported in Figure 6. At 0.0 V, methanol was not observed, as also seen in the FTIR spectrum.

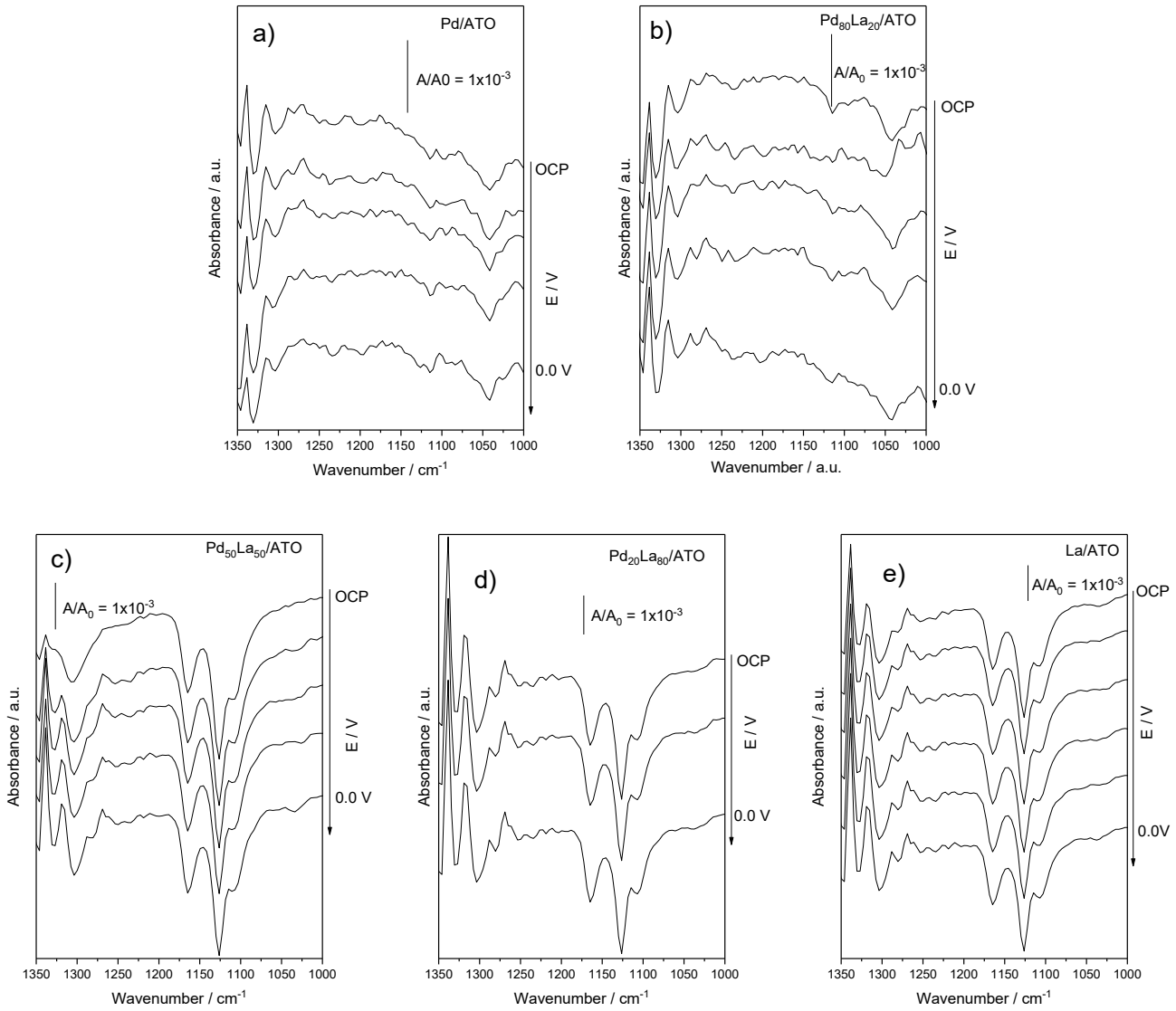

Figure 5. FTIR spectra (**a**–**e**) Spectra of FTIR aliquots obtained from the reactor effluent were collected at intervals of every 100 mV for a duration of 5.0 min in a 1.0 mol L^{-1} NaOH solution, with the methane flow set at 100 mL min^{-1} for all catalysts.

The quantification of produced methanol was carried out using HPLC, and the results were expressed as a reaction rate following Equation (1):

$$r = \frac{\text{Methanol}_{\text{amount}}}{\text{Volume} \times \text{Time}} \quad (1)$$

Figure 6 illustrates the reaction rate for methanol production with Pd- and La-based catalysts supported on ATO. According to the data, the $Pd_{50}La_{50}$/ATO catalyst exhibits higher reaction rates at the potential of 0.0 V, a material that also shows a higher power density, as observed in Figure 4b. However, the $Pd_{80}La_{20}$/ATO and Pd/ATO materials show methanol production rates at various potentials, while La/ATO did not exhibit the presence of methanol. The data indicate that catalysts containing Pd and La in an optimal ratio promote a balance between sites across the material that favors methanol production.

This combination is successful due to the synergy between the water activation capacity from lanthanum and the carbophilic nature of PdO [6,19].

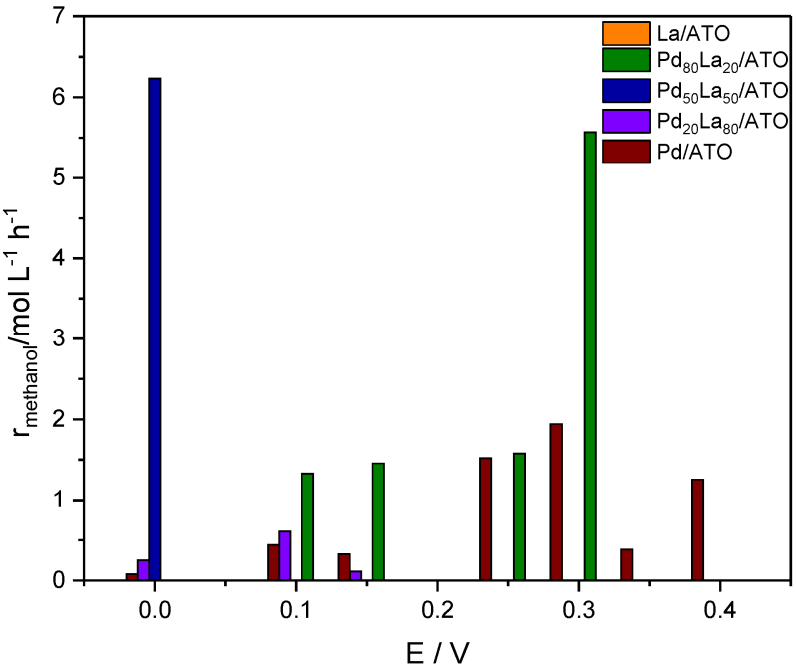

Figure 6. Reaction rate for methanol production calculations were performed using Equation (1) for Pd-La materials at various potentials.

4. Conclusions

The study focuses on the electrochemical conversion of methane to methanol using fuel-cell-type electrochemical reactors with palladium- and lanthanum-based catalysts supported on antimony-doped tin oxide (ATO). The combination of these elements revealed promising features for the selective production of methanol.

Transmission electron microscopy analysis highlighted the influence of lanthanum addition to palladium nanoparticles, affecting the size distribution and clusters. Polarization curves and power density plots underscored the effectiveness of the $Pd_{50}La_{50}$/ATO catalyst, suggesting an optimal relationship between palladium and lanthanum to optimize methanol production. FTIR analysis revealed the presence of methane and methanol in the reaction products, while the methanol production rate highlighted the superior performance of the $Pd_{50}La_{50}$/ATO catalyst compared to other compositions. The synergy between lanthanum's water activation capability and the carbophilic nature of PdO emerged as a crucial factor for the success of this catalyst.

Author Contributions: P.V.R.G.: Methodology. D.R.R.L.: Original draft. G.S.: Investigation. V.A.M.: Investigation. R.F.B.d.S.: Writing, review and editing. A.O.N.: Writing and supervision. All authors have read and agreed to the published version of the manuscript.

Funding: FAPEAM (N.012/2021–POSGFE), CAPES, CNPQ (302709/2020-7, 407967/2022)- for supports.

Data Availability Statement: The original contributions presented in the study are included in the article, further inquiries can be directed to the corresponding authors.

Conflicts of Interest: The authors declare that they have no known competing financial interests or personal relationships that could have appeared to influence the work reported in this paper.

Abbreviations

ATO	Antimony-Doped Tin Oxide
TEM	Transmission Electron Microscopy
XRD	X-ray Diffraction
PEM	Proton Exchange Membrane
FTIR	Fourier-Transform Infrared Spectroscopy
HPLC	High-Performance Liquid Chromatography

References

1. Abdel, R.M.H.; Amin, R.S.; El-Khatib, K.M. Preparation and characterization of Pt–CeO_2/C and Pt–TiO_2/C electrocatalysts with improved electrocatalytic activity for methanol oxidation. *Appl. Surf. Sci.* **2016**, *367*, 382–390.
2. Arnarson, L.; Schmidt, P.S.; Pandey, M.; Bagger, A.; Thygesen, K.S.; Stephens, I.E.L.; Rossmeisl, J. Fundamental limitation of electrocatalytic methane conversion to methanol. *Phys. Chem. Chem. Phys.* **2018**, *20*, 11152–11159. [CrossRef]
3. Blanco, H.; Nijs, W.; Ruf, J.; Faaij, A. Potential of Power-to-Methane in the EU energy transition to a low carbon system using cost optimization. *Appl. Energy* **2018**, *232*, 323–340. [CrossRef]
4. Christensen, P.A.; Linares-Moya, D. The Role of Adsorbed Formate and Oxygen in the Oxidation of Methanol at a Polycrystalline Pt Electrode in 0.1 M KOH: An In Situ Fourier Transform Infrared Study. *J. Phys. Chem. C* **2010**, *114*, 1094–1101. [CrossRef]
5. Cook, R.L.; Sammells, A.F. Ambient Temperature Methane Activation to Condensed Species under Cathodic Conditions. *J. Electrochem. Soc.* **1990**, *137*, 2007. [CrossRef]
6. De Souza RF, B.; Florio, D.Z.; Antolini, E.; Neto, A.O. Partial Methane Oxidation in Fuel Cell-Type Reactors for Co-Generation of Energy and Chemicals: A Short Review. *Catalysts* **2022**, *12*, 217. [CrossRef]
7. De Souza, R.F.B.; Neto, É.T.; Calegaro, M.L.; Santos, E.A.; Martinho, H.S.; Dos Santos, M.C. Ethanol Electro-oxidation on Pt/C Electrocatalysts: An "In Situ" Raman Spectroelectrochemical Study. *Electrocatalysis* **2011**, *2*, 28–34. [CrossRef]
8. Fernandez-Garcia, S.; Jiang, L.; Tinoco, M.; Hungria, A.B.; Han, J.; Blanco, G.; Calvino, J.J.; Chen, X. Enhanced Hydroxyl Radical Scavenging Activity by Doping Lanthanum in Ceria Nanocubes. *J. Phys. Chem. C* **2016**, *120*, 1891–1901. [CrossRef]
9. Hamada, K.; Morishita, H. The Rotation-Vibrational Spectra and Structures of Methanol and Acetonitrile. *Spec-Troscopy Lett.* **1980**, *13*, 15–29. [CrossRef]
10. Lange, J.-P.; Sushkevich, V.L.; Knorpp, A.J.; Van Bokhoven, J.A. Methane-to-Methanol via Chemical Looping: Economic Potential and Guidance for Future Research. *Ind. Eng. Chem. Res.* **2019**, *58*, 8674–8680. [CrossRef]
11. Lei, Y.; Chu, C.; Li, S.; Sun, Y. Methane Activations by Lanthanum Oxide Clusters. *J. Phys. Chem. C* **2014**, *118*, 7932–7945. [CrossRef]
12. Li, X.; Wang, C.; Yang, J.; Xu, Y.; Yang, Y.; Yu, J.; Delgado, J.J.; Martsinovich, N.; Sun, X.; Sheng, X.Z.; et al. PdCu nanoalloy decorated photocatalysts for efficient and selective oxidative coupling of methane in flow reactors. *Nat. Commun.* **2023**, *14*, 6343. [CrossRef]
13. Ma, L.; Chu, D.; Chen, R. Comparison of ethanol electro-oxidation on Pt/C and Pd/C catalysts in alkaline media. *Int. J. Hydrog. Energy* **2012**, *37*, 11185–11194. [CrossRef]
14. Meng, X.; Cui, X.; Rajan, N.P.; Yu, L.; Deng, D.; Bao, X. Direct Methane Conversion under Mild Condition by Thermo-, Electro-, or Photocatalysis. *Chem* **2019**, *5*, 2296–2325. [CrossRef]
15. Mestl, G.; Ruiz, P.; Delmon, B.; Knozinger, H. Sb_2O_3/Sb_2O_4 in reducing/oxidizing environments: An in situ Raman spectroscopy study. *J. Phys. Chem.* **1994**, *98*, 11276–11282. [CrossRef]
16. Muniz-Miranda, M.; Zoppi, A.; Muniz-Miranda, F.; Calisi, N. Palladium Oxide Nanoparticles: Preparation, Characterization and Catalytic Activity Evaluation. *Coatings* **2020**, *10*, 207. [CrossRef]
17. Qu, W.; Wang, Z.; Sui, X.; Gu, D. An efficient antimony doped tin oxide and carbon nanotubes hybrid support of Pd catalyst for formic acid electrooxidation. *Int. J. Hydrog. Energy* **2014**, *39*, 5678–5688. [CrossRef]
18. Ramos, A.S.; Santos MC, L.; Godoi, C.M.; Oliveira Neto, A.; De Souza, R.F.B. Obtaining C2 and C3 Products from Methane Using Pd/C as Anode in a Solid Fuel Cell-type Electrolyte Reactor. *ChemCatChem* **2020**, *12*, 4517–4521. [CrossRef]
19. Santos MC, L.; Nunes, L.C.; Silva LM, G.; Ramos, A.S.; Fonseca, F.C.; De Souza, R.F.B.; Neto, A.O. Direct Alkaline Anion Exchange Membrane Fuel Cell to Converting Methane into Methanol. *ChemistrySelect* **2019**, *4*, 11430–11434. [CrossRef]
20. Shavi, R.; Hiremath, V.; Seo, J.G. Radical-initiated oxidative conversion of methane to methanol over metallic iron and copper catalysts. *Mol. Catal.* **2018**, *445*, 232–239. [CrossRef]
21. Tyagi, S.; Ganesh, A.; Aghalayam, P. Direct Methane Proton Exchange Membrane Fuel Cell. *ECS Trans.* **2019**, *6*, 371–378. [CrossRef]
22. Xie, S.; Lin, S.; Zhang, Q.; Tian, Z.; Wang, Y. Selective electrocatalytic conversion of methane to fuels and chemicals. *J. Energy Chem.* **2018**, *27*, 1629–1636. [CrossRef]

23. Zhong, M.; Xu, Y.; Li, J.; Ge, Z.-X.; Jia, C.; Chen, Y.; Deng, P.; Tian, X. Engineering PdAu Nanowires for Highly Efficient Direct Methane Conversion to Methanol under Mild Conditions. *J. Phys. Chem. C* **2021**, *125*, 12713–12720. [CrossRef]
24. Zhang, M.; Wang, Y.; Ma, Y.; Wang, X.; Zhao, B.; Ruan, W. Study of charge transfer effect in Surface-Enhanced Raman scattering (SERS) byusing Antimony-doped tinoxide (ATO) nanoparticles as substrates with tunable optical band gaps andfree charge carrier densities. *Spectrochim. Acta Part A Mol. Biomol. Spectrosc.* **2022**, *264*, 120288. [CrossRef] [PubMed]